JOURNAL OF AGRICULTURAL AND FOOD CHEMISTRY

Model Applications and Intermediates Quantification of Atrazine Degradation by UV-Enhanced Fenton Process

KWAI-HING CHAN AND WEI CHU*

Department of Civil and Structural Engineering, Research Centre for Environmental Technology and Management, and The Hong Kong Polytechnic University, Hunghom, Kowloon, Hong Kong

Degradation of the herbicide atrazine (ATZ) by the UV-enhanced Fenton process (UV-FP) was investigated. An enhanced photochemical effect was observed in the process compared with the simple combination of the two individual reaction rates of sole-UV (UV radiation) and dark-FP (sole Fenton's process). Accordingly, a photochemical model based on the two parallel reactions was proposed to predict the reaction kinetics of UV-FP, where two rate enhancement factors were adopted and found to be capable of successfully describing the rate improvement. In addition, the transformation pathway of ATZ decay was successfully investigated by using novel technology, liquid chromatography−electrospray tandem mass spectrometry (LC/ESI-MS/MS). Fourteen intermediates were identified in the process. The alkylic oxidation followed by dealkylation and/or dechlorination−hydroxylation was found to be the major pathway of the decay of ATZ in UV-FP. All of the detected intermediates were found to be dealkylated in different levels or positions. The dealkylated species were found to be further dechlorinated. The chlorinated products reduced to 17% of total, whereas the dechlorinated products remained at 73% and were further decayed after 60 min of treatment. In view of the gradual reduction of the mass balance of the total *s*-triazine, this suggested that a ring cleavage may occur on the ATZ in the UV-FP.

KEYWORDS: Atrazine; Fenton; oxidation; radical; ultraviolet

INTRODUCTION

Increasing concerns about the environment have stimulated the development of new wastewater treatment processes that are able to promote the complete mineralization of potentially toxic compounds and which can be feasibly implemented at lower costs. In recent years, advanced oxidation processes (AOP) have been intensively investigated. They are considered to be more promising alternatives than conventional wastewater treatments due to their ability to oxidize a great variety of organic contaminants by the generation of highly oxidative hydroxyl radicals $HO^{\bullet}$ (*1*). UV radiation alone would result in the attack on and decomposition of organic molecules by bond cleavage and free radical generation, but usually it occurs at comparatively slow rates because only direct photolysis was available. The combination of UV light and various oxidants is capable of decomposing pollutants much more effectively. For example, the decomposition of organic pollutants using hydrogen peroxide as an oxidant under UV illumination has been proven to be effective (*2*). Other researchers have worked on the electrochemical Fenton (AFT) process of atrazine (ATZ) and found excellent removal of atrazine and high production of dechlorinated product (*3*).

Among all of the AOPs, the Fenton process (FP) using ferrous salt and hydrogen peroxide has attracted considerable attention due to its high efficiency in generating hydroxyl radicals by decomposing H_2O_2 with the catalyst Fe(II) in an acidic medium, which improves the oxidative rates of less biodegradable organic compounds (*4*). The FP has been widely applied in the treatment of hazardous organic substances, such as phenols and chlorophenols (*5*), industrial wastewater from the dyehouse industry (*6*), pharmaceutical wastewater (*7*), and textile secondary effluents (*8*), and the degradation of the herbicides (*9*).

Recent studies have indicated that the UV-assisted FP (UV-FP, by using $UV/Fe^{2+}/H_2O_2$) can further enhance the decomposition of many refractory organics, such as the applications of landfill leachate (*10*) and the degradation of pesticides (*11*), nitrobenzene and other organics (*12*), chlorobenzenes (*13*), chlorophenols (*14*), dichloromethane (*15*), and dyes (*16*). The enhancement of organic decomposition is likely due to the photolysis of the aqueous complex $Fe(OH)^{2+}$, which provides an additional source of $HO^{\bullet}$ radicals (*8*). In addition, the photolysis of $Fe(OH)^{2+}$ is capable of regenerating Fe^{2+} ions, which indirectly results in the lower requirement of Fe^{2+} dosages in a UV-FP compared with the conventional FP (*12*).

* Author to whom correspondence should be addressed (fax +852-23346389; e-mail cewchu@polyu.edu.hk).

10.1021/jf052572e CCC: $33.50
Published on Web 02/01/2006

The herbicide atrazine [2-chloro-4-(ethylamino)-6-(isopropylamino)-*s*-triazine]

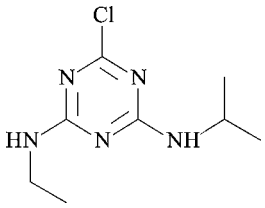

has been used widely to combat weeds in corn and sorghum crops. It is a typical pollutant over which there are environmental concerns because of its low biodegradability and high potential to contaminate surface water and groundwater. Its potential for polluting drinking water has led some countries to ban this herbicide. In addition, it is classified as a possible human carcinogen by the U.S. EPA (*17*). At present, the understanding of reaction kinetics and systematic optimization/prediction of UV-FP in removing chemicals such as ATZ is very limited. In this study, the degradation mechanism of atrazine by UV-FP at a UV wavelength of 253.7 nm is investigated, and a theoretical kinetic model with corrections is derived accordingly. The transformation products of the ATZ decay were investigated and evaluated by using liquid chromatography (LC) together with the electrospray ionization−mass spectrometry (ESI-MS) and tandem mass spectrometry (MS/MS), which separate and directly characterize the reaction products to reveal the degradation mechanism and reaction pathways of the process

METHODOLOGY

Chemicals. All chemicals used were of HPLC grade and were used as received without further purification. Nonlabeled ATZ at 99% purity and its main decay intermediates (which were commercially available) were purchased from RdH Laborchemikalien GmbH & Co. including 2-chloro-4-(isopropylamino)-6-amino-*s*-triazine (CIAT, 99.9%), 2-chloro-4-(ethylamino)-6-amino-*s*-triazine (CEAT, 96.1%), 2-hydroxy-4-(isopropylamino)-6-(ethylamino)-*s*-triazine (OIET, 94.7%), 2-hydroxy-4-(ethylamino)-6-amino-*s*-triazine (OEAT, 95.4%), and 2-hydroxy-4-(isopropylamino)-6-amino-*s*-triazine (OIAT, 98.7%). Acetonitrile (from Labscan Asia Co. Ltd.) was degassed before being used in liquid chromatography (LC). Ferrous salt ($FeSO_4 \cdot 7H_2O$) and H_2O_2 (30% solution) were purchased from RbH and Junsei Chemical Ltd. (Japan), respectively. Sulfuric acid and methanol purchased from Labscan were used to adjust solution pH and prepare quenching solutions, respectively.

Methods. The stock solutions of ATZ, CIAT, CEAT, OIET, OEAT, and OIAT were prepared at 0.116, 0.128, 0.212, 0.05, 0.100, and 0.106 mM, respectively, in HPLC water. The 1 mM Fe(II) was prepared in an acidic solution (pH 2) to prevent the formation of $Fe(OH)_2$ precipitation. A series of batch tests were employed to determine the degradation of ATZ under different [FP] doses, that is, the solution containing the same [Fe(II)] and [H_2O_2] concentration, each at 0.01, 0.05, 0.10, 0.15, and 0.20 mM at a fixed 1:1 ratio. Because the FP is most effective at low pH levels (*18*, *19*) and it is favored to minimize possible errors due to the self-decay of H_2O_2 at elevated pH, the solution pH was adjusted at 2.8 by using H_2SO_4 in this study.

The Fe(II) and H_2O_2 solutions were freshly prepared for each experiment to minimize errors resulting from precipitation and self-decomposition. Predetermined amounts of Fe(II), ATZ, and deionized−distilled water solutions were mixed together in the quartz reactor. H_2O_2 was then added (to reach a final volume of 200 mL), and the photoreactor was turned on simultaneously to initiate the reaction. The mixture was stirred by a magnetic stir bar throughout the reaction to ensure the homogeneity of the solution. For a photoassisted reaction, the experiments were conducted in a Rayonet RPR-200 photochemical reactor system (Supporting Information, Figure 1), manufactured by the Southern New England Ultraviolet Co. The system consisted of a 300 mL cylindrical quartz column with i.d. of 20 mm and phosphor-coated low-pressure mercury lamps. A quartz column was filled with 200 mL of reaction solution and irradiated in the photoreactor. Two 253.7 nm lamps were used as light sources throughout the experiment and were arranged symmetrically within the photoreactor. The light intensity of each lamp was 1.5×10^{-6} Einstein L^{-1} s^{-1}. Samples of 1 mL taken at different retention times were mixed with the same volume of methanol to quench the reaction (*18*). The sample was filtered before analysis by HPLC (by 0.45 μm filter) and ESI-MS/MS (by 0.25 μm filter).

Table 1. Identified Degradation Products and Their Main Fragments Determined by LC/ESI-MS/MS

compound	retention time (min)	$[M + H^+]$	ESI-MS/MS spectrum (*m*/*z*) ions
ATZ	12.43	216	216, 174, 146, 132, 110, 104, 96, 68
met-CMIT	11.92	246	246, 188, 130, 104
CDIT	9.77	230	230, 188, 146, 110, 104, 79, 68
CIAT	8.80	188	188, 146, 110, 104, 79, 68
OIET	8.20	198	198, 156, 128, 114, 86
CEAT	7.45	174	174, 146, 132, 110, 104, 96, 79, 68
CDET	7.38	216	216, 188, 174, 146, 132, 104, 96, 79, 71, 68
OAAT	6.25	128	128, 86
ODIT	6.02	212	212, 170, 128, 86
ODET	6.00	198	198, 170, 156, 128
CDAT	5.60	188	188, 146
ODAT	5.55	170	170, 128, 86
OIAT	5.33	170	170, 128, 86
CAAT	4.82	146	146, 110, 104, 79, 68, 62
OEAT	4.58	156	156, 128, 114, 96, 86, 71

Analytical Methods. *High-Pressure Liquid Chromatography (HPLC).* For the investigation of ATZ degradation, the sample aliquots were collected from different reaction times and analyzed by HPLC. The HPLC, a Finnigan SpectraSYSTEM LC, consisted of a solvent degasser, a quaternary gradient pump, an inert autosampler with a 20 μL injection loop, and a photodiode array UV detector. The chromatographic separations were performed on the stainless steel Restek column: 5 μm 4.6 (i.d.) × 250 mm Pinnacle Octyl Amine column. The maximum absorption wavelength of ATZ was selected as 221 nm (Supporting Information, Figure 2). The mobile phase consisting of 60% acetonitrile with 40% DDW was delivered at a flow rate of 1.5 mL min^{-1}, which resulted in an ATZ peak at 3.5 min. In addition, a five-point calibration curve was run for ATZ with detection limit of 1.59 μM.

Electrospray Ionization Tandem Mass Spectrometry (ESI-MS/MS). The investigation of ATZ's transformation intermediates was performed by HPLC combined with electrospray ionization and tandem mass spectrometry (HPLC/ESI-MS/MS) on a Finnigan ThermoQuest LCQ Duo. The eluent (1 mL min^{-1}) was delivered by a gradient system from HPLC and partitioned by an Alltech (Alltech Associates, Inc.) Hypersil ODS column (C_{18}, 5 μm, 4.6 × 250 mm). The elution was carried out with a gradient flow of from 95 to 0% of ammonia acetate (5 mM, pH 4.6) and from 5 to 89% of acetonitrile, together with 0−11% of water in 15 min. After the analytical run, the column was rinsed with a solution containing 50% methanol and 50% water for 5 min and the mobile phase returned to the initial condition in 5 min. The maximum absorption wavelength of ATZ and its transformation intermediates ranged from 207 to 221 nm. Four-point calibration curves were constructed for ATZ and its transformation products. When standards were not available, the response factors were adapted from compounds of a similar nature (chloro- or hydroxytriazines as determined by the UV spectra) and from the retention times. The LC eluent was then directed to the ESI, and positive ions ($M + H^+$) were detected in the selected reaction monitoring mode. The ESI probe was installed with sheath and auxiliary gases run at 80 and 20 (in arbitrary units), respectively. MS conditions were as follows: capillary temperature, 250 °C; voltage, 46 V; spray voltage, 4.5 kV. The MS/MS experiments were carried out by using helium as the collision gas (30%, 100% collision energy corresponding to 5 V from peak to peak).

The retention time, precursor ($M + H^+$), and MS/MS spectrum ions are listed in **Table 1**. It should be noted that all of the reported CMIT

data in this study were originally from the results of met-CMIT, where the CMIT was transferred into met-CMIT during the quenching by methanol (*20*). In addition, the ODET was found to merge with the ODIT peak in the LC analysis, so the latter was reported in terms of ODET + ODIT based on the MS analysis. Degradation products of the ATZ intermediates were conducted by the stocks from separate tests.

RESULTS AND DISCUSSION

Photodecay of ATZ at Various FP Doses. The decay of 0.01 mM ATZ by FP without the use of UV was investigated in a previous study under different [FP] doses that ranged from 0.01 to 0.20 mM (*21*). It is interesting to note that the data do not follow a pseudo-first-order kinetic as previously suggested by Gallard et al. (*13*, *22*). Instead, a pseudo-second-order kinetic was found to be more suitable to describe the reaction (Supporting Information, Figure 3). After a thorough analysis, the difference in reaction kinetics apparently resulted from the dissimilar ranges of substrate (i.e., ATZ) and reagents [i.e., Fe(II) and H_2O_2] applied in the reactions. At a very high reagent-to-substrate ratio of 10000:1 (in Gallard's case), a pseudo-first-order kinetic was observed. This was because when the concentrations of reagents ([Fe(II)] and [H_2O_2]) are very large compared to that of the substrate (ATZ), the reagent terms can be assumed to remain constant throughout the reaction, so that the reaction rate depended only on [ATZ] and a pseudo-first-order kinetic resulted. As the reagent-to-substrate ratio is comparatively low (e.g., from 1:1 to 20:1 in this study), the variation of reagent concentration can no longer be ignored nor be simplified as constants, which makes the use of a first-order kinetic inappropriate. Similar observations were also reported by Lin and Gurol (*23*) and De Laat and Gallard (*24*). In addition, because the subreactions involved in the chain reactions of FP are mainly of second order (*25*), and the use of a high ratio may not be appropriate in a real application, it is rational to use the pseudo-second-order reaction mechanism in deriving the kinetic model for practical purposes.

Depending on the initial [FP] doses, the ATZ removal could range from about 40 to 98%. It was found that the higher the [FP] concentration, the faster and more extensively the fraction of ATZ was degraded. This suggests that both the Fe(II) and H_2O_2 were consumable during the reaction of FP. In addition, the degradation of ATZ depended on the sufficiency of Fe(II) and H_2O_2 in the FP. To minimize the limitations and to improve the performance of FP, the oxidation of ATZ by FP in the presence of UV radiation was therefore studied. A typical example in degrading 0.01 mM ATZ is shown in **Figure 1**. The dark-FP, using 0.15 mM [FP] (without UV), cannot remove ATZ completely, and the process ceases in 300 s, resulting in a tailing of residual concentration of ATZ. Meanwhile, the sole-UV radiation (without [FP]) has a lower initial decay rate, so an extended irradiation time (~4 times) is required to achieve a conversion similar to that of dark-FP. Nevertheless, ATZ could be rapidly and completely decayed by combining these two systems, that is, a photoassisted Fenton process (UV-FP). As noted in **Figure 1**, >99% of ATZ was removed by the UV-FP system in <200 s and ATZ was not detected after 250 s. In general, UV-FP reduces the reaction time by >87% and improves the ATZ removal by >21% compared with the sole-UV radiation and dark-FP, respectively.

Derivation of the Proposed Kinetic Model. In a previous study, the decay kinetics of ATZ by dark-FP was found to be described by a second-order mechanism (*26*). In addition, the sole-UV was observed to follow pseudo-first-order with respect to ATZ concentration (data not shown). If a synergistic effect

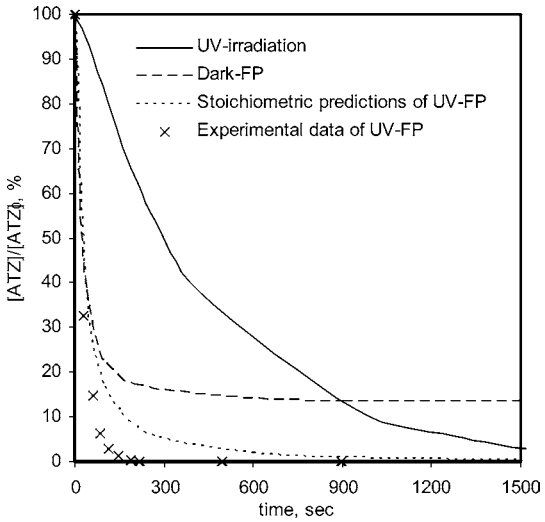

Figure 1. Stoichiometric predictions of the UV-FP with FP doses at 0.15 mM.

Table 2. Values of k_2 in Different FP Doses

[FP] (mM)			
[Fe(II)]	[H_2O_2]	k_2 (mM^{-1} s^{-1})	r^2
0.01	0.01	0.17	0.671
0.05	0.05	0.75	0.944
0.10	0.10	2.15	0.996
0.15	0.15	3.64	0.985
0.20	0.20	8.91	0.896

results from the combination of the two systems, UV-FP can theoretically consist of two parallel irreversible first- and second-order reactions. The differential equations of sole-UV and dark-FP are

$$\frac{dC}{dt} = -k_1 C \quad (1)$$

$$\frac{dC}{dt} = -k_2 C^2 \quad (2)$$

where C is the concentration of the organic substrate (ATZ) in the system in mM and t is the reaction time in seconds. k_1 and k_2 are rate constants for sole-UV and FP, respectively, and have been solved by linearizing eqs 1 and 2. k_1 is 0.0023 s^{-1} under the light intensity of 3×10^{-5} Einstein L^{-1} s^{-1} at 253.7 nm, and the values of k_2 were evaluated and are listed in **Table 2** at different [FP] doses.

The rate law of a parallel system consists of sole-UV, and dark-FP results by combining eqs 1 and 2 mathematically, so the concentration of ATZ in the UV-FP is

$$\frac{dC}{dt} = -k_1 C - k_2 C^2 \quad (3)$$

By substituting $C = 1/\epsilon$

$$\frac{d\epsilon}{dt} = k_2 + k_1 \epsilon \quad (4)$$

Solving eq 4 by multiplying $e^{-k_1 t}$

$$\frac{d}{dt}(\epsilon\, e^{-k_1 t}) = k_2\, e^{-k_1 t} \quad (5)$$

$$\epsilon\, e^{-k_1 t} = -\frac{k_2}{k_1} e^{-k_1 t} + \gamma \quad \text{(where } \gamma \text{ is a constant)} \qquad (6)$$

Thus, the ATZ concentration in the proposed model can be solved as

$$C = \frac{1}{\epsilon} = \frac{k_1}{-k_2 + k_1 \gamma\, e^{k_1 t}} \quad \text{and} \quad \gamma = \frac{k_1 + k_2 C_0}{C_0 k_1} \qquad (7)$$

where γ was solved by using the initial ATZ concentration, C_0, at $t = 0$.

On the basis of eq 7, the stoichiometric predictions of ATZ decay in UV-FP were obtained and are illustrated in **Figure 1** for comparison. It is not surprising to note that the proposed model underestimated the performance of the combined system as well as the decay of ATZ. This interesting result is likely due to the oversimplification of the model, in which was not included a synergistic photochemical term incorporating sole-UV and FP species. Hence, the photochemical enhancement should be quantified and incorporated into the proposed UV-FP model, so that the modified model can be used to predict the overall performance of UV-FP in real applications by incorporating factors that correspond to the levels of the photochemical effect.

Accordingly, the original rate law (eq 3) was restated by incorporating the two rate constants k_1 and k_2 by such factors to reflect the photochemical effect:

$$\frac{dC}{dt} = -\alpha k_1 C - \beta k_2 C^2 \qquad (8)$$

The solution of the corrected model therefore could be derived as

$$C = \frac{\alpha k_1}{-\beta k_2 + \alpha k_1 \gamma\, e^{\alpha k_1 t}} \quad \text{and} \quad \gamma = \frac{\alpha k_1 + \beta k_2 C_0}{C_0 \alpha k_1} \qquad (9)$$

where α and β are the respective photochemical factors of k_1 and k_2, and they can be easily solved by the following approaches: (i) determine the constant γ by initial condition, (ii) assign two arbitrary reaction times (t_1 and t_2), (iii) substitute those known variables (C_1, C_2, k_1, k_2, γ, t_1, and t_2) into eq 9, and (iv) solve the two equations. Thus, the database of α and β can be constructed on the basis of eq 9.

The predicted values derived from the original (eq 7) and modified (eq 9) models are compared with the experimental data as shown in **Figure 2**. The data demonstrate that the proposed photochemical factors can correct the original model and describe the observed experimental data successfully. Therefore, the decay of ATZ by UV-FP at various reaction conditions were investigated, and it was seen that the higher the [FP] dose in the UV-FP, the faster the decay rate of ATZ and the shorter the completion time (see **Figure 3**). The data were also fitted to the modified model, and the results were incorporated in **Figure 3**, where the model could predict the ATZ decay in UV-FP accurately with the help of photochemical factors α and β.

Analysis of Rate Enhancement Factors. Referring to the modified model, a further analysis of the rate enhancement factors α and β was necessary for prediction purposes. By solving eq 9, the respective factors α and β were obtained for each set of UV-FP with various [FP] concentrations, and the results are plotted in **Figure 4**. It was found that α and β are

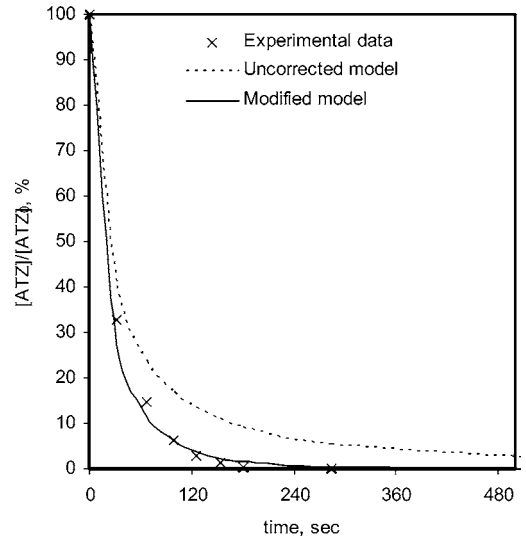

Figure 2. Modeling on the degradation of ATZ by the UV-FP with FP dose at 0.15 mM. The experimental data can be fitted well into the model after modification.

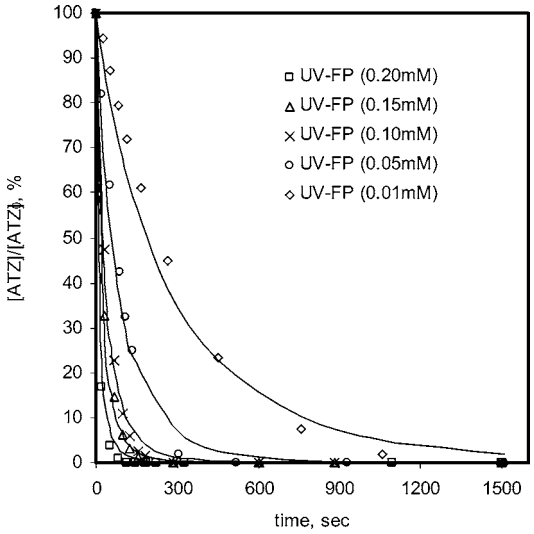

Figure 3. Modified UV-FP model well describes the experimental data. The solid lines indicate the model in different FP doses.

highly dependent on [FP], for which linear relationships with R^2 of 0.9933 and 0.9960 are identified. The mathematical expressions of these factors are

$$\alpha = 39.71[\text{FP}] + 1 \qquad (\alpha \geq 1) \qquad (10)$$

$$\beta = 1.00[\text{FP}] + 1 \qquad (\beta \geq 1) \qquad (11)$$

Mathematically speaking, both eqs 10 and 11 have positive slopes and a common intercept of 1 (i.e., they are always higher than unity), indicating that the involvement of α and β in the treatment process will always improve the decay rate of ATZ. In addition, as the [FP] is decreased, the corresponding values of α and β approach 1 and the photochemical effect vanishes. The agreements between the experimental observations and mathematical equations indicate that the use of the photochemical effect to elucidate rate enhancement is supported.

The rate enhancement effect apparently resulted from the interactions between light irradiation with the FP species [i.e., H_2O_2 and Fe(II)], which included the following: (1) an increase in the formation rate of hydroxyl free radicals ($HO^{\bullet}$) through a

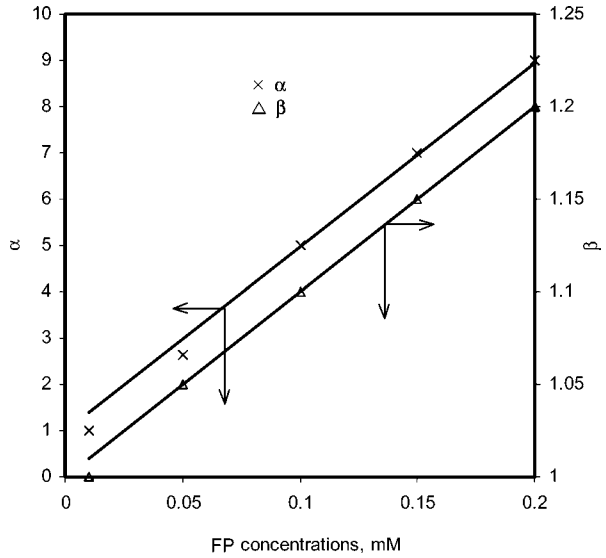

Figure 4. Linear relationships of α and β with FP concentrations (from eq 8).

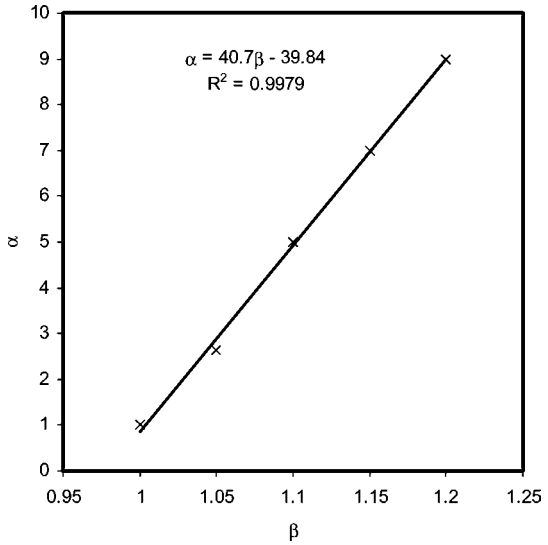

Figure 5. Linear relationships between α and β.

parallel pathway of direct photolysis of H_2O_2 when the wavelength of UV is <360 nm (*25*)

$$H_2O_2 \xrightarrow{h\nu} 2HO^{\bullet} \quad (12)$$

and (2) the regeneration of catalyst Fe(II) and associated free radicals from the spent Fe(III) in the presence of sole-UV (*27*)

$$Fe^{3+} + H_2O \xrightarrow{h\nu} Fe^{2+} + H^+ + HO^{\bullet} \quad (13)$$

$$Fe^{3+}(L^-) \xrightarrow{h\nu} Fe^{2+} + L^{\bullet} \quad (L = \text{organic ligand}) \quad (14)$$

It should be noted that the involvement of radicals of organic ligand (e.g., $RCOO^-$, RO^-, RNH^+, etc.) in eq 14 was suggested as being a more efficient way to oxidize organic substrates than via $HO^{\bullet}$ (*3*).

Applications of the UV-FP Process. It was also found that the two photochemical factors have a linear correlation as shown in **Figure 5** (with an R^2 of 0.9979), which makes it possible to simplify the design procedures of UV-FP by merging eqs 10 and 11 and **Figure 7** into a correlation plot (see **Figure 6**), so that the design parameters such as α, β, and k_2 can be quickly

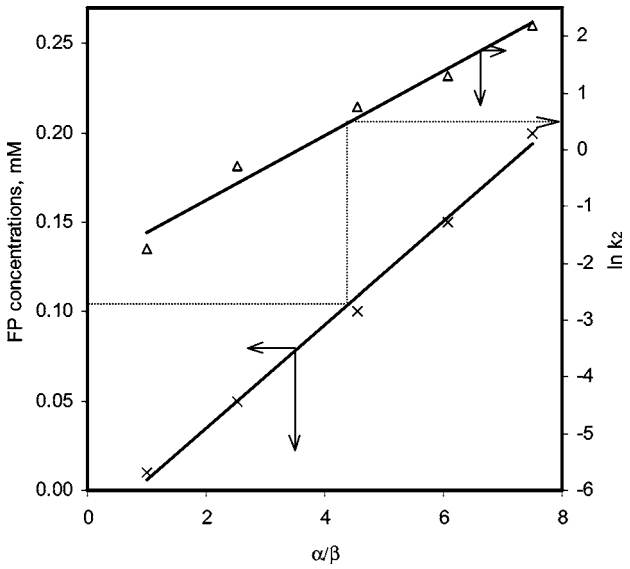

Figure 6. Intercorrelation of FP doses, α, β, and rate constant k_2.

determined in one step with any given [FP] concentration. A typical example is illustrated in **Figure 6**, where the term α/β ratio is used to differentiate the contributions of the photochemical effect from two different sources (i.e., UV process and FP). It is interesting to note that the higher the [FP] dose, the higher the α/β ratio, which implies that increasing [FP] will improve the rates of both sole-UV and dark-FP in the system but at different levels. According to eq 8, the rate enhancement factors, α and β, reflect the rate improvement on the sole-UV (eq 1) and FP (eq 2). A sensitivity analysis of α and β therefore was conducted to verify such a difference between α and β.

By examining the initial ATZ decay rate in terms of normalized $\Delta C/\Delta t$ at various conditions, a three-dimensional plot of the corresponding α and β values can be resolved in different FP concentrations ranging from 0.20 to 0.01 mM, as shown in **Figure 7**. Referring to eq 8, it is interesting to find that the change of initial rates $\Delta(\Delta C/\Delta t)$ is linearly correlated to the variation of α and β, so the marginal effects of α and β to the change of initial rates [i.e., $\partial(\Delta C/\Delta t)/\partial\alpha$ and $\partial(\Delta C/\Delta t)/\partial\beta$] can be quantified. Thus, the following partial differentiation equations with respect to α and β can be obtained:

$$\frac{\partial}{\partial\alpha}\left(\frac{dC}{dt}\right) = -k_1 C \quad (15)$$

$$\frac{\partial}{\partial\beta}\left(\frac{dC}{dt}\right) = -k_2 C^2 = -f([\text{COP}])C^2 \quad (16)$$

Referring to eq 15, the sensitivity of α to k_1 is 0 as constant light intensity was used in this study. On the other hand, the sensitivity of β to k_2 is clearly dependent on the function of [FP] (eq 16). These verified the observation in **Figure 8**.

The rate enhancement of α is maintained at a constant 2.6×10^{-5} s^{-1} regardless of [FP], whereas the rate enhancement of β is sensitive and increased with the change of [FP]. Because there is evidence that α is normally higher than β among the tested [FP] ranges, the mechanisms of the photochemical effect in the UV-FP system are shown.

(1) First, the presence of UV can greatly increase the concentrations of $HO^{\bullet}$ and $L^{\bullet}$ (eqs 12 and 14), which offers an additional channel for ATZ decay. Because the lifetime of the involved free radicals is extremely short, the steady-state approximation of their concentrations is often valid (*28*). The radical term in the kinetic expression can be integrated into the

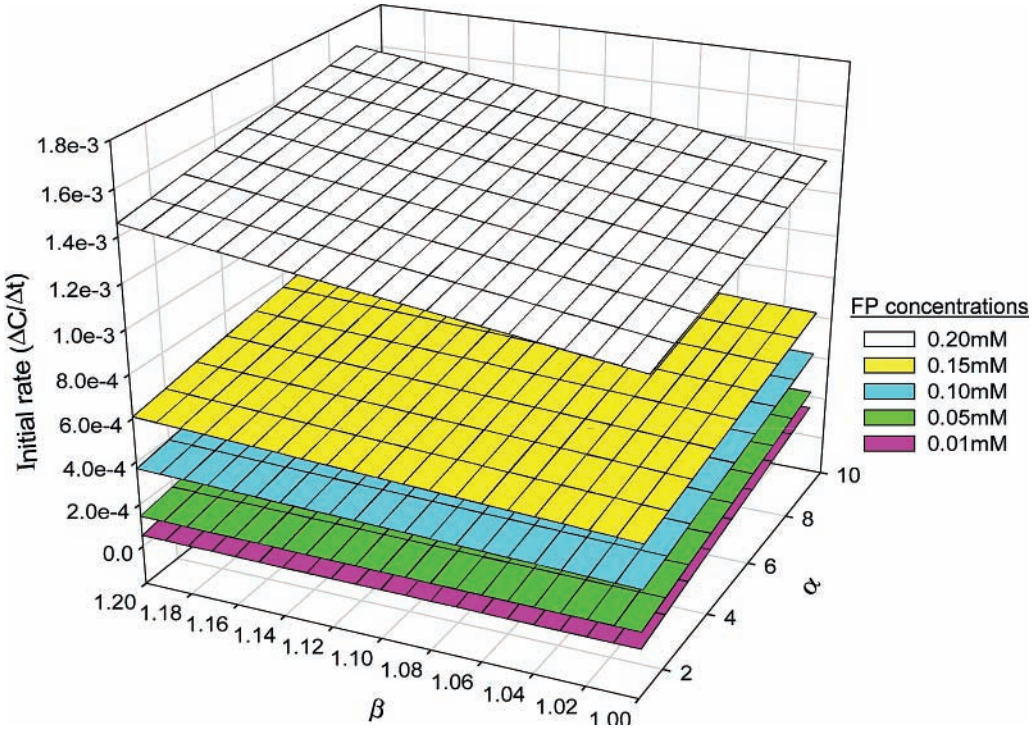

Figure 7. Sensitivity analysis on the decay rate with α and β (from top to bottom, FP = 0.20, 0.15, 0.10, 0.05, and 0.01 mM).

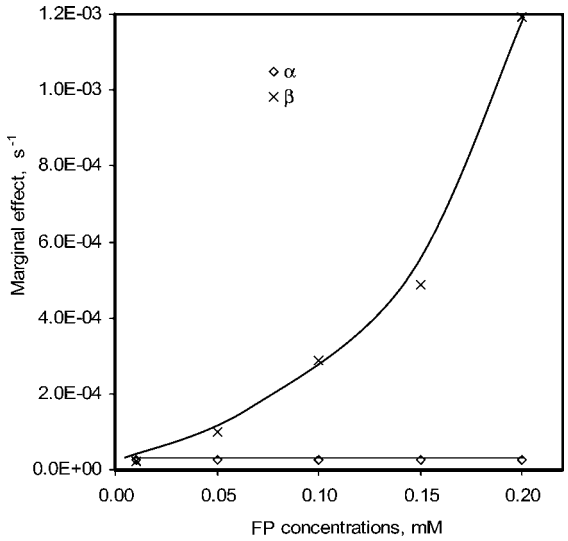

Figure 8. Differential changes of decay rate with α are independent of FP concentrations; however, the change of decay rate with β is sensitive to FP doses.

rate constant. The oxidation of ATZ by such additional radicals can be characterized as a pseudo-first-order process with an overall rate constant of $k_{radical}$, especially if the radical has resulted from a UV reaction (*29*). Therefore, a reverse derivation of eq 8 shows that if another pseudo-first-order term due to the additional free radical oxidation is added, it will naturally merge with the original UV process (which is also a pseudo-first-order process) and result in a high α value as we observed.

$$\frac{dC}{dt} = -\alpha k_1 C - \beta k_2 C^2 = -(k_1 + k_{radical})C - \beta k_2 C^2 = -k_1 C - k_{radical} C - \beta k_2 C^2 \quad (17)$$

(2) The rate enhancement effect of β significantly increased with the increase of [FP], which can be reasonably be explained by the dependence of FP on the doses of [Fe(II)] as previously suggested by Bigda (*30*). At low [FP], the decay of ATZ is limited to the low catalyst concentration of [Fe(II)], which becomes a rate-limiting step to the process and results in a lower ATZ decay rate. However, as the FP dose increases, the [Fe(II)] is likely no longer going to be the rate-limiting step, and the presence of UV will simultaneously accelerate the regeneration of [Fe(II)] (see eqs 13 and 14). As a result, a higher than unity and an upward concave curve of rate enhancement effect of β are observed.

(3) Although the marginal effect of β is significantly higher than that of α, the α/β ratio still increases with [FP], suggesting that the rate enhancement effect contributed by the increment of [Fe(II)] is minor (it can also be justified by a close to 1 rate β value), and the reaction acceleration due to the radical generation induced by UV is more dominant.

Decay Mechanism of ATZ by the UV-FP Process. The process mechanism that resulted by combining sole-UV and dark-FP for the degradation of ATZ was investigated under the same reaction conditions (0.1 mM [FP] with [I] at 3.06×10^{-6} Einstein L^{-1} s^{-1} UV intensity at 253.7 nm). Because of the "compound effect", as discussed previously, the generation of extra radicals apart from those in the original sole-UV and dark-FP resulted in more complicated degradation pathways in connections of the decay pathways and suggests the enhanced synergism between sole-UV and dark-FP. Resulting from the intensified radical supply and continuous UV radiation in UV-FP, 14 degradation intermediates were identified (see **Table 2**). The transformation/degradation pathways were organized and are shown in **Figure 9**. The intermediates were categorized into primary, secondary, and tertiary intermediates, and all of them were sorted by chlorinated or dechlorinated products. In the process, the major oxidant was the $HO^{\bullet}$, because $HOO^{\bullet}$ and its conjugate base $O_2^{\bullet -}$ were much less reactive than hydroxyl radicals (*26*, *31*, *32*). The presence of $HO^{\bullet}$ initiated the decay of ATZ through alkylic oxidation (alkylamino side chain oxidation), dealkylation (alkylic side chain cleavage), and/or dechlorination (hydroxylation at the chlorine site) and generated

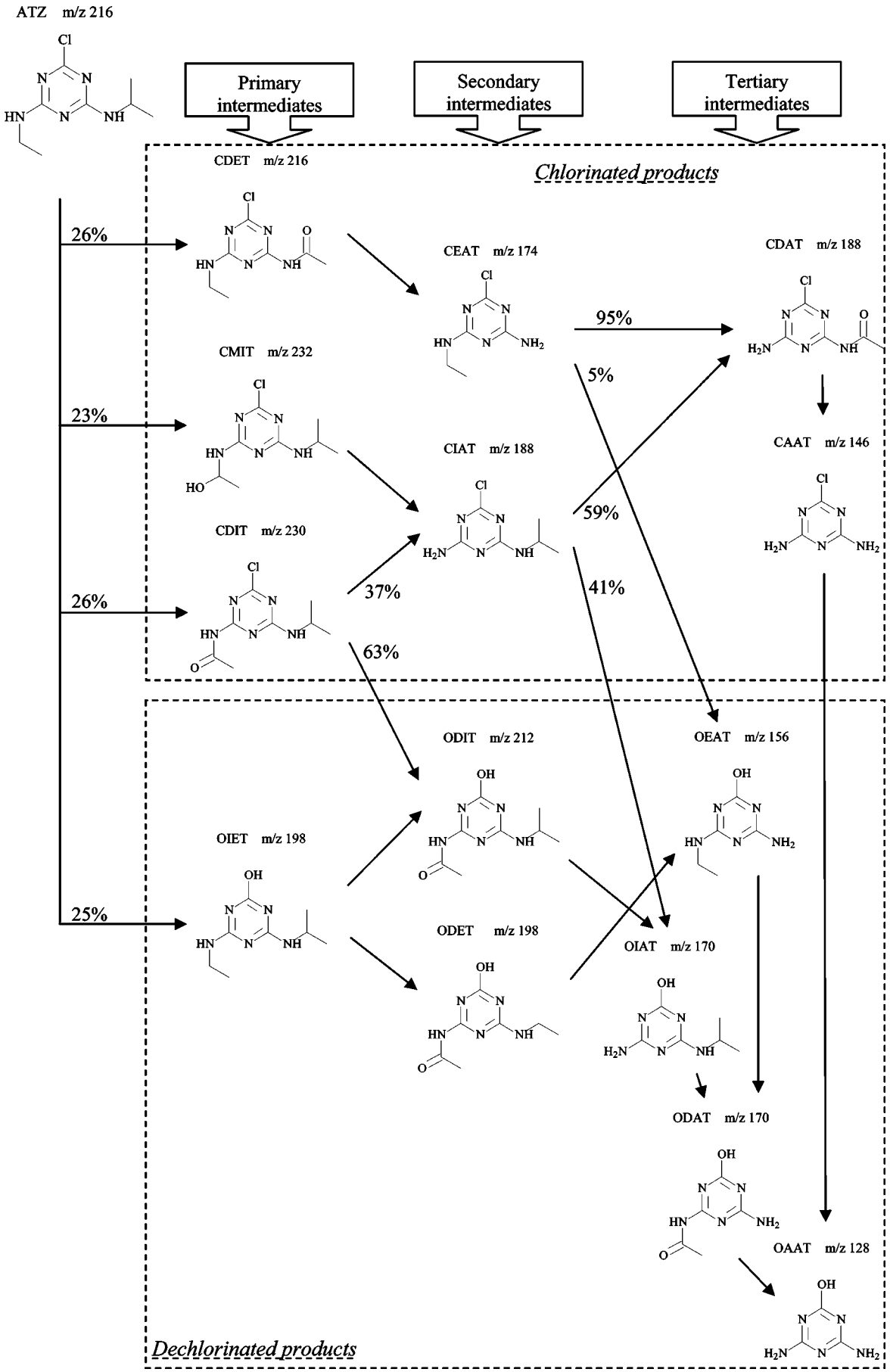

Figure 9. Degradation pathways of ATZ. Percentages (at 350 s of reaction time) given are the relative importance of a pathway (no indications mean 100%).

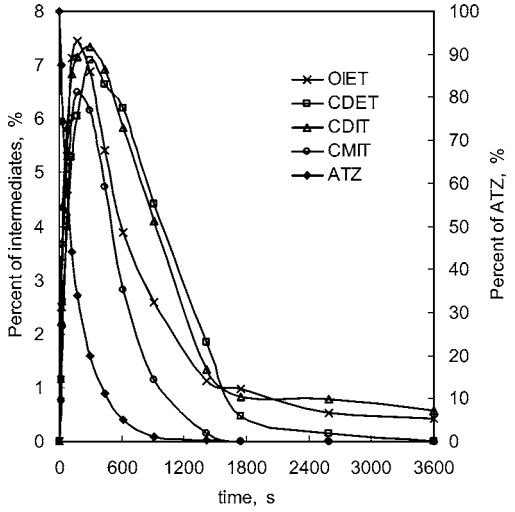

Figure 10. Degradation profile of ATZ to the primary intermediates (i.e., OIET, CDET, CDIT, and CMIT).

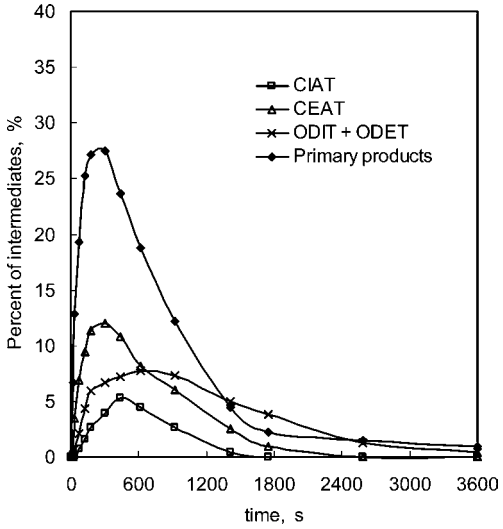

Figure 11. Degradation profile of the primary intermediates to the secondary intermediates (i.e., CIAT, CEAT, ODIT, and ODET).

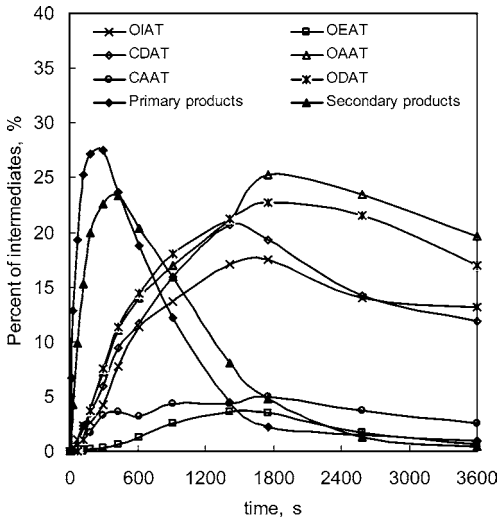

Figure 12. Degradation profile of the primary intermediates and secondary intermediates to OIAT, OEAT, CDAT, OAAT, CAAT, and ODAT.

the corresponding intermediates. Dealkylation may be initiated by the abstraction of a hydrogen atom (H) from the secondary carbon atom (C) of the ethylamino side chain, producing a free radical (eq 18) (*18*), which resulted in the subsequent production of various intermediates.

$$HO^{\bullet} + RNHCH_2CH_3\ (\equiv ATZ) \rightarrow H_2O + RNHC^{\bullet}HCH_3 \quad (18)$$

Dechlorination−hydroxylation could be initiated by an HO• attack of the *s*-triazine ring at the C−Cl position, resulting in an oxidation of the aromatic heterocyclic ring (of ATZ), whereas hydroxylation occurred simultaneously, so that the chlorine atom was substituted by a hydroxyl group. Hence, various hydroxylated *s*-triazines formed in the solution.

In **Figure 10**, the rise of concentrations of three chlorinated and one dechlorinated primary intermediates CDET, CMIT, CDIT, and OIET (26, 23, 26, and 25%, respectively, at 350 s of reaction time) in the beginning of reaction suggested that the decay of ATZ was mainly initiated by alkylic oxidation instead of dechlorination−hydroxylation. Then, the dealkylation of CDET yielded CEAT, followed by another alkylic oxidation to form CDAT and a dechlorination−hydroxylation to form OEAT in the next 200 s (**Figures 9**−**13**). This suggested that both alkylic oxidation and dechlorination−hydroxylation on CEAT might occur simultaneously. This was confirmed by conducting a separate test on CEAT in UV-FP, where CDAT and OEAT were found to be the primary products of CEAT. A similar reaction was also observed on CDIT and CMIT. Their decay subsequently yielded CIAT and ODIT, which was then followed by the formation of CDAT and OIAT. This was mostly similar to the profiles of CDIT and to the decay of CMIT in dark-FP (verified by running a separating test on dark-FP). The exception was that OAAT was observed in the dark-FP instead of OIAT in UV-FP. This is a very interesting finding as the OAAT was previously reported to be the dealkylation product of ODIT (*18*). In a previous study, it was found that only one dechlorinated product, OIET, was observed in the sole-UV, and three dechlorinated products, OIET, ODIT, and OAAT at very low concentration, were observed in the dark-FP (*26*). The lack of detailed information between ODIT and OAAT in the dark-FP was possibly due to the inefficient process and low (undetectable) intermediate concentrations. The direct transformation from ODIT to OAAT is unlikely to take place, due to the low probability of double dealkylation occurring simultaneously on both amino side chains. However, in UV-FP, the concentrations of missing intermediates were boosted by the more powerful process, and OIAT and ODAT were detected as the stepwise dealkylated derivatives in the solution. The formation of CDAT and OIAT from CIAT was confirmed by running a separate test. Thus, similar to the decay of CEAT, both the alkylic oxidation and dechlorination−hydroxylation of CIAT were observed for the decay mechanism of CIAT.

On the other hand, the corresponding molecular structures and a separate test of the degradation of OIET, a sequential transformation from OIET to ODIT and ODET (via alkylic oxidation) and then to the OIAT and OEAT, respectively (via dealkylation), was proposed. Compared with dark-FP and sole-UV, [OIET] was found to be much higher and could be further degraded, which suggested that the photochemical effect improved the performance of the degradation of ATZ in UV-FP, especially for the generation of dechlorinated products. A new tertiary intermediate identified in UV-FP was ODAT, which resulted from the alkylic oxidation of OIAT and OEAT. In addition, a high [OAAT] was observed at the end of the process, which was the dechlorination−hydroxylation product of CAAT (see the profiles in **Figure 12**). In **Figure 12**, the full removal of ATZ in UV-FP followed precisely by a serial transformation

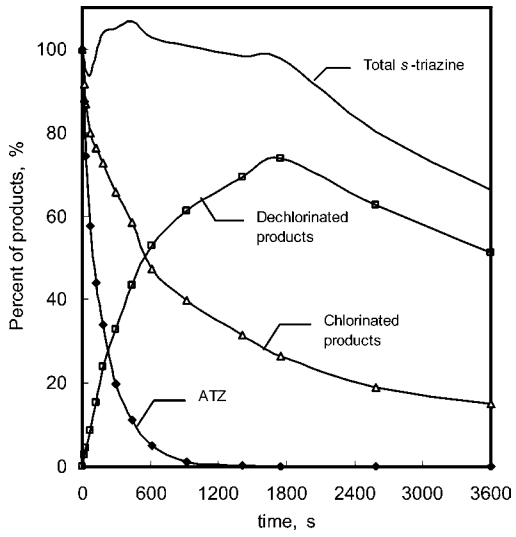

Figure 13. Comparison of chlorinated and dechlorinated products of the degradation of ATZ by UV-FP.

of primary, secondary, and then tertiary products can be observed. This supported the accuracy of the proposed mechanisms in **Figure 9**. The transformation of ATZ and its intermediates (in terms of chlorinated and dechlorinated products) and the mass balance (in *s*-triazine) in UV-FP are incorporated in **Figure 13**. According to this figure, the process successfully remediated not only the parent compound, ATZ, but also its chlorinated intermediates produced during the process. Thus, dechlorinated products were observed accordingly. In view of the mass balance of the total *s*-triazine (percent), the decreasing *s*-triazine fraction suggested that ring cleavage in UV-FP may be possible. Because the H_2O_2 together with its photochemical effect (with UV) was theoretically depleted in the early stage of UV-FP, the degradation of all of the *s*-triazine in the solution at the later stage should have been contributed by "sole-UV-radiation" (the only available energy source driving the process). Besides the possible ring cleavage occurring in UV-FP, the drop of the mass of the total *s*-triazine may be partly due to the undetectable intermediates from the LC-MS. It is interesting to note that the common primary intermediate, OIET, which cannot decay further in the sole-UV-radiation (verified by running a separate test), has been oxidized and then dealkylized in UV-FP. These findings provide solid support that the use of dark-FP together with UV radiation (i.e., UV-FP) is mutually beneficial and can successfully overcome some process obstacles that could not be individually accomplished before.

In conclusion, the UV-enhanced Fenton process was found to be a useful way to accelerate the decay of the herbicide atrazine compared to the sole-UV and dark-FP processes. In addition, a photochemical effect was observed, and a proposed model resulting from the combination of sole-UV and FP was successfully developed to describe the reaction kinetics of UV-FP. Two rate enhancement factors based on the sole-UV and dark-FP processes were derived and investigated in detail. The evidence showed that the mechanism of the rate enhancement effect is mainly dominated by the generation of free radicals that were induced by UV, and the contribution of rate improvement resulting from the dark-FP is less significant. The transformation mechanism of ATZ degradation by UV-FP was successfully investigated. Fourteen intermediates were identified. The degradation pathways of ATZ were evaluated. It was found that alkylic oxidation followed by dealkylation and dechlorination−hydroxylation was likely the major pathway. Additionally, ring cleavage occurred on the ATZ.

ABBREVIATIONS USED

[ATZ], concentration of atrazine (mM); $[ATZ]_0$, concentration of atrazine at the beginning of reaction (mM); $[ATZ]_b$, concentration of atrazine at the break point of the two phases (mM); b_1, rate constant in phase I ($mM^{-1}\ s^{-1}$); b_2, rate constant in phase II ($mM^{-1}\ s^{-1}$); CAAT, 2-chloro-4,6-diamino-*s*-triazine; CDAT, 2-chloro-4-acetamido-6-amino-*s*-triazine; CDET, 2-chloro-4-acetamido-6-(ethylamino)-*s*-triazine; CDIT, 2-chloro-4-acetamindo-6-(isopropylamino)-*s*-triazine; CEAT, 2-chloro-4-(ethylamino)-6-amino-*s*-triazine; CIAT, 2-chloro-4-(isopropylamino)-6-amino-*s*-triazine; CMIT, 2-chloro-4-(1-methylethanolamino)-6-(isopropylamino)-*s*-triazine; met-CMIT, 2-chloro-4-(1-carboxylethanolamino)-6-(isopropylamino)-*s*-triazine; dark-FP, Fenton's process without UV radiation; DDW, distilled−deionized water; ESI-MS/MS, electrospray ionization tandem mass spectrometry; F/H ratios, Fe(II) to H_2O_2 ratios; [Fe(II)], concentration of ferrous ion (mM); FP, Fenton's process; HPLC, high-pressure liquid chromatography; $[H_2O_2]$, concentration of hydrogen peroxide (mM); I_b, *y*-intercept of the plot of ln b_1 against ln b_2; I_r, *y*-intercept of the plot of ln b_1 against F/H ratio; i.d., internal diameter; $[M + H^+]$, positive ions; OAAT, ammeline, 2-hydroxy-4,6-diamino-*s*-triazine; ODAT, 2-hydroxy-4-acetamido-6-amino-*s*-triazine; ODET, 2-hydroxy-4-acetamido-6-(ethylamino)-*s*-triazine; ODIT, 2-hydroxy-4-acetamindo-6-(isopropylamino)-*s*-triazine; OEAT, 2-hydroxy-4-(ethylamino)-6-amino-*s*-triazine; OIAT, 2-hydroxy-4-(isopropylamino)-6-amino-*s*-triazine; OIET, 2-hydroxy-4-(isopropylamino)-6-(ethylamino)-*s*-triazine; sole-UV, irradiation by UV; *t*, reaction time (s); t_b, break point time (s); UV, ultraviolet; UV-FP, UV-assisted Fenton process.

Supporting Information Available: Views of photochemical reactor, absorption spectra of ATZ, and degradation of ATZ. This material is available free of charge via the Internet at http://pubs.acs.org.

LITERATURE CITED

(1) Legrini, O.; Oliveros, E.; Braun, A. M. Photochemical processes for water treatment. *Chem. Rev.* **1993**, *93*, 671−698.

(2) Hirvonen, A.; Tuhkanen, T.; Kalliokoski, P. Treatment of TCE- and PCE-contaminated graoundwater using UV/H_2O_2 and O_3/H_2O_2 oxidation processes. *Water Sci. Technol.* **1996**, *33*, 67−73.

(3) Saltmiras, D. A.; Lemley, A. T. Atrazine degradation by anodic Fenton treatment. *Water Res.* **2002**, *36*, 5113−5119.

(4) Pignatello, J. J.; Liu, D.; Huston, P. Evidence for an additional oxidant in the photoassisted Fenton reaction. *Environ. Sci. Technol.* **1999**, *33*, 1832−1839.

(5) Trapido, M.; Veressinina, Y.; Munter, R. Advanced oxidation processes for degradation of 2,4-dichloro- and 2,4-dimethylphenol. *J. Environ. Eng.* **1998**, *124*, 690−694.

(6) Ruppert, G.; Bauer, R.; Heisler, G. UV-O_3, UV-H_2O_2, UV-TiO_2 and the photo-Fenton's comparison of advanced oxidation processes for wastewater treatment. *Chemosphere* **1994**, *28*, 1447−1454.

(7) Höfl, C.; Sigl, G.; Specht, O.; Wurdack, I.; Wabner, D. Oxidative degradation of AOX and COD by different advanced oxidation processes: a comparative study with two samples of pharmaceutical wastewater. *Water Sci. Technol.* **1997**, *35*, 257−264.

(8) Kang, S. F.; Chang, H. M. Coagulation of textile secondary effluents with Fenton's reagent. *Water Sci. Technol.* **1997**, *36*, 215−222.

(9) Pignatello, J. J. Dark and photoassisted Fe^{3+}-catalyzed degradation of chlorophenoxy herbicides by hydrogen peroxide. *Environ. Sci. Technol.* **1992**, *26*, 944−951.

(10) Kim, S. M.; Geissen, S. U.; Vogelpohl, A. Landfill leachate treatment by a photoassisted Fenton reaction. *Water Sci. Technol.* **1997**, *35*, 239−248.
(11) Fallmann, H.; Krutzler, T.; Bauer, R. Applicability of the photo-Fenton method for treating water containing pesticides. *Catal. Today* **1999**, *54*, 309−319.
(12) Yang, M.; Hu, J.; Ito, K. Characteristics of Fe^{2+}/H_2O_2/UV oxidation process. *Environ. Sci. Technol.* **1998**, *19*, 183−191.
(13) Gallard, H.; De Laat, J. Kinetic modelling of Fe(III)/H_2O_2 oxidation reactions in dilute aqueous solution using atrazine as a model organic compound. *Water Res.* **2000**, *34*, 3107−3116.
(14) Benitez, F. J.; Beltran-Heredia, J.; Acero, J. L. Oxidation of several chlorophenolic derivatives by UV irradiation and hydroxyl radicals. *J. Chem. Technol. Biotechnol.* **2001**, *76*, 312−320.
(15) Feitz, A. J.; Guan, J.; Chattopadhyay, G. Photo-Fenton degradation of dichloromethane for gas-phase treatment. *Chemosphere* **2002**, *48*, 401−406.
(16) He, J.; Tao, X.; Ma, W. H. Heterogeneous photo-Fenton degradation of an azo dye in aqueous H_2O_2/iron oxide dispersions at neutral pHs. *Chem. Lett.* **2002**, *1*, 86−87.
(17) Belluck, D. A.; Benjamin, S. L.; Dawson, T. In *Pesticide Transformation Products: Fate and Significance in the Environment*; Somasundaram, L., Coats, J. R., Eds.; ACS Symposium Series 459; American Chemical Society: Washington, DC, 1991; pp 254−273.
(18) Arnold, S. M.; Hickey, W. J.; Harris, R. F. Degradation of atrazine by Fenton's reagent: condition optimization and product quantification. *Environ. Sci. Technol.* **1995**, *29*, 2083−2089.
(19) Sun, Y.; Pignatello, J. J. Chemical treatment of pesticide wastes: evaluation of Fe(III) chelates for catalytic hydrogen peroxide oxidation of 2,4-D at circumneutral pH. *J. Agric. Food Chem.* **1992**, *40*, 322−327.
(20) Nélieu, S.; Kerhoas, L.; Einhorn, J. Degradation of atrazine into ammeline by combined ozone/hydrogen peroxide treatment in water. *Environ. Sci. Technol.* **2000**, *34*, 430−437.
(21) Chan, K. H.; Chu, W. Modeling the reaction kinetics of Fenton's process on the removal of atrazine. *Chemosphere* **2003**, *51*, 305−311.
(22) Gallard, H.; De Laat, J. Kinetic of oxidation of chlorobenzenes and phenyl-ureas by Fe(II)/H_2O_2 and Fe(III)/H_2O_2. Evidence of reduction and oxidation reactions of intermediates by Fe(II) or Fe(III). *Chemosphere* **2001**, *42*, 405−413.
(23) Lin, S. S.; Gurol, M. D. Catalytic decomposition of hydrogen peroxide on iron oxide: kinetics, mechanisms, and implications. *Environ. Sci. Technol.* **1998**, *32*, 1417−1423.
(24) De Laat, J.; Gallard, H. Catalytic decomposition of hydrogen peroxide by Fe(III) in homogeneous aqueous solution: mechanism and kinetic modeling. *Environ. Sci. Technol.* **1999**, *32*, 2726−2732.
(25) Jones, C. W. *Applications of Hydrogen Peroxide and Derivatives*; Royal Society of Chemistry: Cambridge, U.K., 1999; pp 44−45.
(26) Chan, K. H.; Chu, W. Model applications and mechanism study on the degradation of atrazine by Fenton's system. *J. Hazard. Mater.* **2005**, *118*, 227−237.
(27) Horváth, O.; Stevenson, K. L. *Charge-Transfer Photochemistry of Coordination Compounds*; VCH Publishers: New York, 1993.
(28) Espenson, J. H. *Chemical Kinetics and Reactions Mechanisms*; McGraw-Hill: New York, 1981; pp 140−143.
(29) Chu, W. Photodechlorination mechanism of DDT in UV/surfactant system. *Environ. Sci. Technol.* **1999**, *33*, 421−425.
(30) Bigda, R. J. Consider Fenton's chemistry for wastewater treatment. *Chem. Eng. Prog.* **1995**, *91*, 62−66.
(31) Bielski, B. H. J.; Cabelli, D. E.; Arudi, R. L. Reactivity of H_2O_2/O_2-radicals in aqueous solution. *J. Phys. Chem. Ref Data* **1985**, *14*, 1041−1100.
(32) Frimer, A. A. In *Oxygen Radicals in Biology and Medicine*; Simic, M. G., et al., Eds.; Plenum Press: New York, 1988; pp 29−38.

Received for review October 18, 2005. Revised manuscript received January 2, 2006. Accepted January 4, 2006. The work described in this paper was supported by a grant from the University Research Fund of the Hong Kong Polytechnic University (GV-952).

JF052572E